Title

HVEM Studies of the Sintering of MgO Nanocrystals Prepared by Mg(OH){sub 2} Decomposition

Authors

Thangaraj, N.
Westmacott, K.H.
Dahmen, U.

Publication Date

1990-02-01

LBL-28653

Lawrence Berkeley Laboratory
UNIVERSITY OF CALIFORNIA

Materials & Chemical Sciences Division

National Center for Electron Microscopy

Presented at the 3rd Conference on Frontiers of
Electron Microscopy in Materials Science,
Oak Brook, IL, May 20–24, 1990, and
to be published in the Proceedings

HVEM Studies of the Sintering of MgO Nanocrystals Prepared by $Mg(OH)_2$ Decomposition

N. Thangaraj, K.H. Westmacott, and U. Dahmen

May 1990

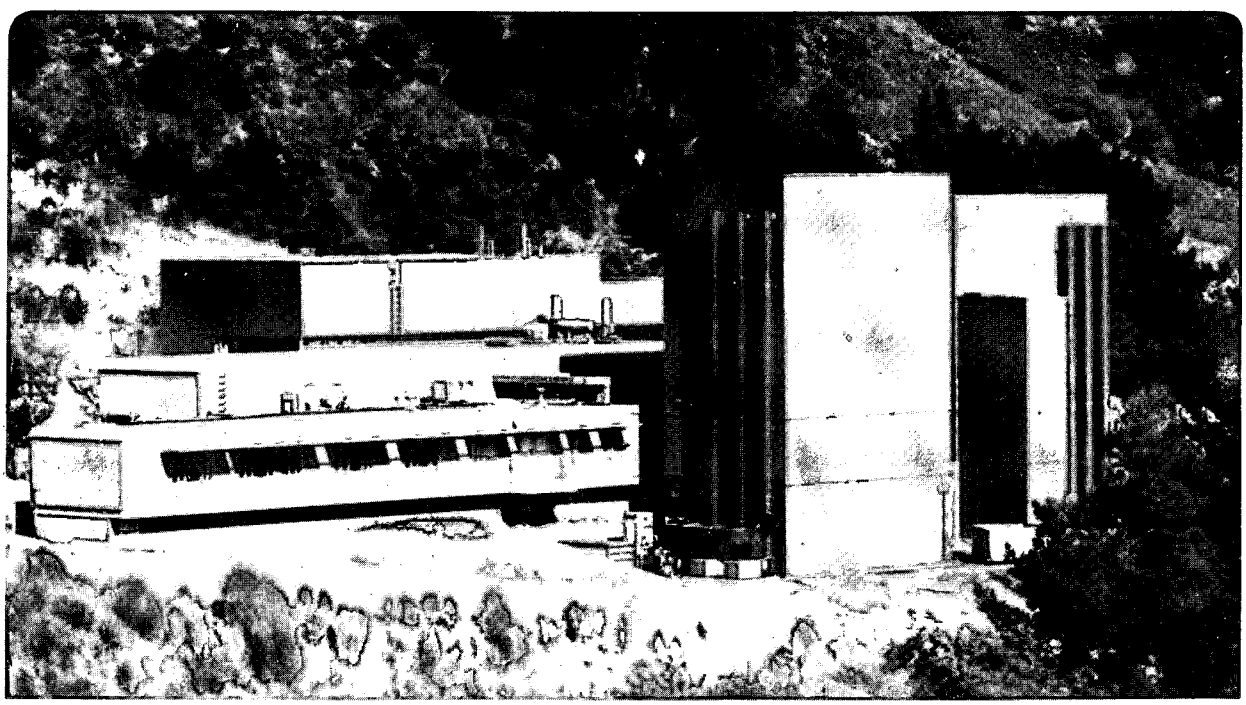

Prepared for the U.S. Department of Energy under Contract Number DE-AC03-76SF00098.

DISCLAIMER

LBL-28653

HVEM STUDIES OF THE SINTERING OF MgO NANOCRYSTALS PREPARED BY $Mg(OH)_2$ DECOMPOSITION

N. Thangaraj, K.H. Westmacott and U. Dahmen

National Center for Electron Microscopy
University of California, Lawrence Berkeley Laboratory
Berkeley, CA. 94720

To be published in Ultramicroscopy as proceedings of the 3rd Conference on Frontiers of Electron Microscopy in Materials Science, Oak Brook, Illinois, May 20-24, 1990.

This work was supported by the Director, Office of Energy Research, Office of Basic Energy Sciences, Material Sciences Division of the U.S. Department of Energy under Contract No. DE-AC03-76SF00098.

HVEM STUDIES OF THE SINTERING OF MgO NANOCRYSTALS PREPARED BY $Mg(OH)_2$ DECOMPOSITION

N. Thangaraj, K. H. Westmacott and U. Dahmen

National Center for Electron Microscopy
Lawrence Berkeley Laboratory
University of California
Berkeley, CA 94720

ABSTRACT

Hot-stage high voltage electron microscopy (HVEM) combined with high resolution electron microscopy (HREM) has been employed to study the microstructural evolution during in-situ decomposition of thin $Mg(OH)_2$ flakes and during early stage sintering of the resultant nanocomposite.The decomposition reaction is known to be pseudomorphic and topotactic, resulting in a regular composite of highly aligned nearly cubic MgO nanocrystals interspersed with a roughly equal volume of pores.This structure was characterized by selected area and optical diffraction techniques as well as by HREM, depending on its microstructural scale. Immediately after decomposition and in the early stages of sintering the fine scale and regular, nearly periodic nature of the microstructure gave rise to diffuse small angle diffraction rings that could be used as a measure of coarsening during in-situ heating in the temperature range 350-900°C. Consistent results were obtained from electron diffraction, optical diffraction and Fourier transforms of digitized images. These measurements were complementary to direct imaging by HREM or conventional imaging techniques.

1. INTRODUCTION

In ceramic processing a suitable selection of heat treatment and precursor material is necessary to obtain good quality dense products. Control over powder characteristics such as crystallite size, shape, and distribution is important. Magnesium oxide (MgO) is a good model material for study because of its technical importance and the wealth of information available in the literature regarding its preparation, transformation from the precursor materials and sintering behavior. Most commercial MgO is obtained from the decomposition of magnesium hydroxide ($Mg(OH)_2$). Several transformation mechanisms for the decomposition behavior of $Mg(OH)_2$ have been proposed (1-4) and the product phase MgO has been studied by x-ray and thermodynamic techniques (5-10). The information obtained from these techniques has been mainly indirect, though some early transmission electron microscopy (TEM) studies provided direct information regarding the relationships between the particle size, shape of the precursor $Mg(OH)_2$ and its calcination product MgO (1,11).

Recently, extensive TEM work was carried out to elucidate the microstructural evolution during the decomposition of $Mg(OH)_2$ and magnesium carbonate ($MgCO_3$). These studies resulted in a detailed picture of transformation morphologies of MgO obtained from the decomposition of $Mg(OH)_2$ and $MgCO_3$ (12,13), the orientation relationships between the parent and product phases (13,14) and the pore and crystallite stacking in the product phase (12,14). The pseudomorphic decomposition of $Mg(OH)_2$ produces highly aligned, approximately cubic crystals of MgO with 2 ± 0.2 nm average edge length (15). The ~50% volume change is accommodated as fine pores dispersed between the MgO crystallites. Since the crystallites as well as the pores are of nanometer scale, the decomposition product may be termed a nanocomposite. To quantify the size, shape, orientation and distribution of crystallites and pores in this type of composite, x-ray line broadening is usually employed. X-ray line broadening techniques fail to provide satisfactory results for the analysis of highly oriented MgO crystallites (16). On the other hand, TEM techniques can be effectively employed to accurately measure the crystallite size and shape at high spatial resolution (17). Using small angle scattering information obtained from the electron diffraction patterns, Watari et al. (18) quantified the microstructural features, identified to be voids in a highly twinned matrix, during the decomposition of goethite (α-FeOOH) to hematite (α-Fe_2O_3) and diaspore (α-AlOOH) to corundum (α-Al_2O_3). Recently, it has been shown that small angle electron or optical diffraction may be used as a complementary technique to measure microstructural characteristics in oriented MgO nanocomposites (19).

Since nanocrystalline MgO has a very high surface area of ~700 m^2/ g (10), it is highly active, and shows unusual behavior that points to high sinterability at low temperatures, similar to that found for other nanocrystalline materials (20). It has further been found that impurities and atmosphere have a strong effect on the sintering behavior of MgO (22-25). Although the initial stages of MgO sintering have been studied extensively by indirect methods, the present paper reports the first direct in-situ HVEM study of this phenomenon.

2. MATERIALS AND EXPERIMENTAL METHODS

The $Mg(OH)_2$ used in this study was prepared by the method used by Moodie and Warble (12). 99.99% pure Aldrich MgO was rehydrated by adding it to boiling distilled water. The beaker containing the hot suspension was then tightly sealed with a Parafilm™ to prevent the formation of carbonate. Storage for 10 days allowed the hydroxide crystals to grow to a size suitable for electron microscopy. TEM samples were prepared by dispersing a drop of the suspension on a 200-mesh copper or molybdenum grid coated with a thin holey carbon film. The crystals usually had a hexagonal plate morphology with a size and thickness ranging from 0.3 to 1 μm and 0.1 to 0.2 μm respectively. Most of the crystals deposited on the grids had their c-axis aligned with the electron beam. However, crystals in other orientations were also observed without tilting the sample.

The electron microscopy was carried out in a JEOL 200CX microscope operated at 200 kV, a Kratos high voltage microscope operated at 1500 kV and the JEOL ARM operated at 800 kV. Hot-stage experiments were conducted either with a 750°C double-tilt stage or with a water cooled 1000°C single-tilt stage. Dynamical events during high temperature in-situ annealing were recorded with a Westinghouse high resolution TV camera and video recording system. Optical diffraction experiments were performed in an optical bench with a He-Ne laser using TEM negatives recorded typically at magnifications of about 80K. Accurate measurement of diffraction patterns was carried out at the NCEM computer facility using an Eikonix digitizing camera and the Semper image processing software.

3. RESULTS AND DISCUSSION

(a) As-decomposed microstructure

The thermal decomposition of $Mg(OH)_2$ has been the subject of extensive investigation (for review, see e.g. 26).The transformation is pseudomorphic, i.e the external shape of the parent $Mg(OH)_2$ is maintained during conversion to the product MgO. The volume change due to the loss of H_2O amounts to ~50% and is accommodated by the formation of a high density of small pores. In spite of this large volume change the transformation is topotactic, and the parent and product phases maintain a simple orientation relationship of parallel close-packed planes and directions, i.e, (13,14)

$(111)\ MgO \parallel (0001)\ Mg(OH)_2$

$[10\bar{1}]\ MgO \parallel [11\bar{2}0]\ Mg(OH)_2$.

Thermal decomposition of $Mg(OH)_2$ occurs at low temperatures (around 300°C), but the transformation can also be carried out and followed in the TEM by simply focussing the electron beam on the specimen.

Fig. 1 shows a typical micrograph of a completely decomposed $Mg(OH)_2$ crystal seen in an edge-on position. The c-axis of the original $Mg(OH)_2$ crystal is perpendicular to the straight edges. During the dehydration process, the water vapor leaves the $Mg(OH)_2$ lattice along channels perpendicular to the c-axis. The water channels and some exfoliation are clearly visible in fig. 1. It is evident from this micrograph that the ~2.5 nm spacing of inter-layer water channels perpendicular to the c-axis is larger than the spacing of the fine, equiaxed inter-particle pores.

Fig. 2a shows a micrograph of partially decomposed $Mg(OH)_2$ crystal oriented along the [0001] zone axis. It was observed that the electron-beam-induced transformation starts at the edge of the crystal and proceeds towards the center. This is seen in fig. 2a where the untransformed $Mg(OH)_2$ at the center of the crystal has a dark diffraction contrast, whereas the transformed crystal near the perimeter exhibits mottled contrast. A typical electron diffraction pattern obtained from such a crystal is shown in fig. 2b. Note that the diffraction spots from $Mg(OH)_2$ are very sharp compared to the MgO spots which are arced and broad. The arcing is due to a slight misorientation between MgO crystallites whereas the broadness originates in the small crystallite size. The spot broadening is illustrated in Fig. 2c in a radial line trace of the diffraction spots arrowed in fig. 2b. Compared to the sharp $(2\bar{1}\bar{1}0)$ $Mg(OH)_2$ peak, the the shape broadening of the (422) MgO peak is clearly evident. The crystallite size can be estimated from the spot dimensions to be about 1 nm.

The completely transformed $Mg(OH)_2$ crystal (fig. 2d) shows a microstructure with highly mottled contrast. To enhance the contrast the image was recorded at a slight underfocus.

This microstructure gives rise to a single crystal diffraction pattern such as the <111> MgO zone axis pattern shown in fig. 2e. It is interesting to note that in addition to the broad and arced MgO spots, small angle scattering is visible as a diffuse ring pattern near the transmitted beam. The diameter and the shape of the diffuse ring were found to depend on crystal orientation. It was hypothesized that this was a result of the regularity and fine scale of the microstructure. If confirmed, this small angle scattering effect could be used to help quantify the microstructure and its evolution in the early stages of sintering.

First, it was established that the mottled contrast visible in low magnification out-of-focus bright field images of the decomposed microstructure (fig. 2d) was related to occurrence of the low-angle scattering; By using such a micrograph as a diffraction grating in an optical diffractometer, a small angle diffraction ring was obtained (see fig. 2f) which may be compared with the corresponding electron diffraction ring seen near the transmitted beam in fig. 2e. It was found that the intensity and broadness, but not the peak diameter, of this optical diffraction ring depended on the defocus of the micrograph used as the grating. No such dependence was of course found for the small angle scattering in electron diffraction patterns. Direct recording of the small angle ring in electron diffraction patterns was difficult due to its close proximity to the transmitted spot, especially for relatively coarse microstructures. A special surface developing technique (27) was therefore used to separate the intensity of the diffuse ring from that of the transmitted beam. Even with this developing technique it remained difficult to measure the diffuse rings directly in electron diffraction patterns. Optical diffraction, or its digital analog, Fourier transformation of a digitized image of the microstructure, were therefore used interchangeably with electron diffraction, especially for small diameters of the diffraction ring (coarser microstructures).

Having determined that the low-angle scattering carries useful information about the microstructure, an attempt was made to quantify this information. An accurate measure of the small angle ring spacing was obtained by averaging over 360 individual line scans taken across the ring diameter at 1° intervals. The resulting plot of diffracted intensity versus diffraction angle is shown in fig. 3a. This line trace was smoothed and differentiated twice to locate the peak intensity. This second derivative is shown in fig. 3b. Using the (220) lattice spacing of MgO as an internal standard, the peak diameter of the ring was found to correspond to 2.2 nm. According to Babinet's principle of optical reversibility, x-ray or electron scattering would be identical if the projected potential of the two phases (particles and pores) were interchanged. The small angle ring is thus equally representative of the particles and the pores. In a fixed volume, changing the shape or distribution of the

particles will change the shape and distribution of the pores in a reciprocal manner. It is therefore the combined effect of particles and pores that is reflected in the diffraction ring. The peak diameter of the ring is inversely proportional to the microstructural parameter λ which corresponds to the average spacing between particles (or pores).

Due to anisotropy of the microstructure the shape of the small angle diffraction ring varies with crystal orientation. This is illustrated in fig. 4. The [111], [110] and [100] zone axes diffraction patterns of MgO nanocrystals are shown in figs. 4a, 4c and 4e respectively. Enlargements of the region around the transmitted beam showing the small angle diffraction rings for the [111], [110] and [100] zones are given in figs.4b, 4d and 4f respectively. It is clearly visible from this figure that the shape of the small diffraction ring changes with the orientation of the MgO. The shape of the ring along these directions corresponds to the projected shape of cube-shaped MgO nanocrystals (and pores) along the respective directions.

(b) Annealed microstructure

To understand the initial stage sintering of MgO nanocrystals, microstructural changes were followed during in-situ heating at 700 and 900°C. Fig. 5 shows a series of electron micrographs of MgO pseudomorphs recorded during annealing at 700°C. The near-hexagonal morphology of the as-decomposed crystal in [0001] orientation is shown in fig. 5a. The fine mottled contrast characteristic of the completely decomposed hydroxide is clearly visible inside the crystal. The remaining micrographs in the figure show the microstructures after 90 min b), 280 min c) and 480 min d) of annealing at 700°C. It is evident that the mottled contrast progressively coarsens during annealing and the external shape of the original $Mg(OH)_2$ crystal is retained even after annealing for a long time. Measurements of MgO microstructural coarsening were carried out using the small angle diffraction ring as described above. The second derivatives of the averaged line profiles of the small angle diffraction rings recorded from the as-decomposed and the annealed sample (480 min at 700°C) are shown superimposed on the digitized ring patterns in figs. 6a and 6b respectively. Values for the microstructural parameter λ increased from 2.2 nm in the as-decomposed sample to 3 nm after annealing for 480 min at 700°C. However, when we made measurements on the averaged line profiles (fig. 7) of power spectra obtained from the digitized images characterizing each coarsening stage (the crystal was constantly under the electron beam during the course of observation) as shown in fig. 5, the microstructural parameter λ shows higher values, e.g. 13.7 nm for the one annealed for 480 min at 700°C.

In other words, the microstructures show enhanced coarsening. This is due to the combined effect of temperature and electron beam effects which will be discussed in the later section.

Selected area diffraction patterns were obtained from similarly sized crystals in the annealed sample for different crystal orientations. As expected, the shrinkage of the small angle diffraction ring confirms the growth of crystallites and pores in the annealed microstructure. The [110] and [100] zone axes diffraction patterns also show shrinkage of the small angle diffracted rings. Furthermore, the ring shapes remain anisotropic.

Fig. 8 shows a sequence of micrographs recorded after different annealing times at 900°C. Again, the $Mg(OH)_2$ crystal in [0001] orientation immediately after decomposition is shown in fig. 8a for comparison. Figs. 8b, c and d show the same crystal annealed at 900°C for 40 min, 90 min and 120 min, respectively. Compared with the behavior at 700°C, the microstructural coarsening at 900°C (fig. 8) is clearly enhanced. The mottled contrast seen in fig. 8a disappeared within 90 minutes of annealing at 900°C, and fine triangular crystals of MgO appeared in the pseudomorph (see fig. 8c). Further annealing caused the triangular crystals to grow and at some later point new crystals with cubic morphology nucleated and grew. A portion of the video recording showing the growth of cube shaped MgO particle is given in fig. 9. The average line profiles (fig.10) obtained from the images shown in fig. 8, again clearly show the decrease in the peak spacing which in turn corresponds to the growth of MgO nanocrystallites and pores. By comparing the line profiles obtained from the images recorded during annealing at 700°C (fig.7) and 900°C (fig.10), enhanced microstructural coarsening at 900°C is clearly evident.

High resolution electron microscopy was employed to observe the crystallite sizes and shapes directly. Figs. 11a and 11b show images of MgO nanocrystallites in [100] projection for the as-decomposed crystal and the one annealed at 700°C for 480 minutes, respectively. Figs. 12a and 12b show similar images in [110] projection. Due to unavoidable overlap, the size of the individual crystallites is not easily measured in these images. However, after annealing the crystallites show better alignment than in the as-decomposed crystal. This was also seen as reduced arc width in the diffraction patterns. The arc width measured from the (200) diffraction spots of MgO recorded from the annealed sample (480 min at 700°C) gives smaller value (~ 9°) than the one obtained from the as-decomposed sample which gives ~15° arc width. Optical diffraction patterns (insets)

obtained from these HREM images show much clearly the decrease in the arc width for the annealed sample compared to the as-decomposed sample.

c) Effect of impurities

Impurities play a major role in the sintering behavior of MgO nanocrystals. The effect of various impurities such as Mn and Fe (22, 23), Na (11), Cl (24) and the influence of different atmospheres such as reducing, oxidizing (23) and water vapor (25) have been studied extensively. As a general rule, all the investigators reported that impurities enhance surface diffusion and surface area reduction and thus promote crystal growth. Furthermore, it has been suggested that water vapor promotes the elimination of closed pores and enhances the growth of open pores and crystals by a surface step mechanism, but not by surface diffusion (25).

During the course of the present investigation it has been found that at 900°C Cu impurities from the specimen support grid cause the MgO pseudomorphs to disintegrate. Video recordings show that nanocrystals break away from the pseudomorph, spheroidize and migrate across the substrate. The particles coarsen by coalescence with other migrating nanocrystals. The larger particles produced by coalescence develop facets. Fig. 13a shows a micrograph taken from a region where one can see disintegrating MgO pseudomorphs with a fine mottled contrast, small triangular shaped MgO crystals and an angular linked particle which is shown by an arrow. Fig. 13b shows a region adjacent to the one in fig. 13a. In this region, the particles have been formed by migration of MgO nanocrystals from the disintegrating MgO pseudomorphs. Occasionally, diffraction evidence indicated the presence of pure copper particles.

These observations suggest that Cu impurities catalyze the disintegration of MgO pseudomorphs. This agrees with earlier reports that additives such as magnesium chloride promote the destruction of the decomposition product and aid the growth MgO crystals (24). It is interesting to note that when a Mo grid was used as a support, even though the presence of other impurities such as Cr, Mo, Fe and Ni was detected, no disintegration of the pseudomorphs was found at 900°C (see fig. 8).

d) Electron Beam Effects

During the course of the present HVEM study it was found that the sintering behavior was influenced by the electron beam. Crystallites kept under observation throughout an annealing run sintered at a faster rate than ones observed intermittently or only at the end of annealing. This effect which is illustrated in fig. 14 is not unexpected since MgO remains an insulator even at 850°C and its thermal conductivity decreases with increasing temperature. Thus electron beam heating is likely to increase the temperature of those crystallites under continuous observation. However, it should be emphasized that significant coarsening occurred at both 700 and 900°C even in the absence of beam effects.

4. CONCLUSIONS

1) Direct in-situ observations are useful for investigating the microstructural changes that occur during the decomposition of $Mg(OH)_2$ and during subsequent sintering of the product MgO nanocomposite.

2) Conventional and high resolution imaging, electron and optical diffraction methods can be used in a complementary manner to characterize the microstructure and monitor its changes quantitatively .

ACKNOWLEDGEMENTS

The authors wish to thank M. A. O'Keefe and J. H. Turner for their help in image processing. This work was supported through Exploratory Research Funds by the Director, Office of Energy Research, Office of Basic Energy Sciences, Materials Sciences Division of the U. S. Department of Energy under Contract No. DE-ACO3-76SFOOO98.

REFERENCES

1. J. F. Goodman, Proc. Roy. Soc. (London), **A247** (1958) 346.
2. M. C. Ball and H. F. W. Taylor, Mineral. Mag., **32** (1961) 754.
3. R. S. Gordon and W. D. Kingery, J. Am. Ceram. Soc., **49** (1966) 654.
4. O. Chaix-Pluchery, J. Bouillot , D. Ciosmak, J. C. Niepce and F. Freund, J. Solid State Chem., **50** (1983) 247.
5. S. Iwai, H. Morikawa, T. Watanabe and H. Aoki, J. Am. Ceram. Soc., **53** (1970) 355.
6. I. F. Guilliatt and N. H. Brett, Phil. Mag., **21** (1970) 671.
7. I. F. Guilliatt and N. H. Brett, Phil. Mag., **23** (1971) 647.
8. D. T. Livey, B. M. Wankyln, M. Hewitt and P. Murray, Trans. Br. Ceram. Soc., **56** (1957) 217.
9. M. Natarajan, T. S. Sharma, J. C. Ahluwalia and C. N. R. Rao, Trans. Faraday Soc., **65** (1969) 3088.
10. D. Beruto, P. F. Rossi and A. W. Searcy, J. Phys. Chem., **89** (1985) 1695.
11. V. A. Phillips, H. Opperhauser and J. L. Kolbe, J. Am. Ceram. Soc., **61** (1978) 75.
12. A. F. Moodie and C. E. Warble, J. Cryst. Growth, **74** (1986) 89.
13. M. G. Kim, U. Dahmen and A. W. Searcy, J. Am. Ceram. Soc., **70** (1987) 146.
14. U. Dahmen, M. G. Kim and A. W. Searcy, Ultramicroscopy, **23** (1987) 365.
15. M. G. Kim, U. Dahmen and A. W. Searcy, J. Am. Ceram. Soc., **71** (1988) C373.
16. M. G. Kim, M. J. Cima and A. W. Searcy, J. Am. Ceram. Soc., **72** (1989) 1514.
17. P. Gallezot, M. Avalos-Borja, H. Poppa and H. Heinemann, Langmuir, **1** (1985) 342.
18. F. Watari, P. Delavignette and S. Amelinckx, J. Solid State Chem., **29** (1979) 417.
19. U. Dahmen and K. H. Westmacott, LBL Report, 1989.
20. J. Eastman and R.W. Siegel, Research and Development, Jan 1989, 56.
21. G. W. Nieman, J. R. Weertman and R. W. Siegel, Scripta Met., **23** (1989) 2013.
22. I. F. Guilliatt and N. H. Brett, Trans. Br. Ceram. Soc., **69** (1970) 1.
23. I. F. Guilliatt and N. H. Brett, J. Chem. Soc. Faraday Trans. I, **68** (1972) 429.
24. K. Hamano, Z. Nakagawa and H. Watanabe, in: Advances in Ceramics, Ed. W. D. Kingery, **10** (1984) 610.
25. D. Beruto, R. Botter and A. W. Searcy, J. Am. Ceram. Soc., **70** (1987) 637.
26. J. Green, J. Mater. Sci., 18 (1983) 637.
27. J. H. Turner and K. M. Krishnan, J. Electron Microsc. Tech., **5** (1987) 711.

FIGURE CAPTIONS

Fig. 1: A typical micrograph of a completely decomposed $Mg(OH)_2$ crystal seen in edge-on position.

Fig. 2: a) An image of partially decomposed $Mg(OH)_2$ crystal oriented along [0001] zone axis. b) Selected area diffraction pattern obtained from the crystal similar to the one shown in fig. a showing the spots due to $Mg(OH)_2$ crystal and MgO nanocrystals. c) Line trace obtained from the diffraction spots shown by an arrow in fig.b. displaying the relative sharpness of the peaks. d) The microstructure of $Mg(OH)_2$ crystal shown in fig. a after completely decomposed to MgO showing fine mottled contrast due to the porous microstructure. e) [111] zone axis diffraction pattern of MgO shows a small angle diffracted ring close to the transmitted spot arising from pores and MgO nanocrystals. f) An optical diffraction pattern recorded from the microstructure of a completely decomposed $Mg(OH)_2$ crystal.

Fig. 3: a) A line scan obtained from the small angle diffracted ring shown in fig. 2e. b) The resulted profile of fig. a after smoothing and differenciating.

Fig. 4: The diffraction patterns of MgO nanocrystals obtained for various crystal orientations showing the shape change of small angle diffracted rings. Diffraction patterns of [111] a), [110] c), [100] e) zone axes and b), d), f) the respective enlarged regions around the transmitted beam.

Fig. 5: Shows microstructures of a same MgO pseudomorph in [111] orientation, annealed at 700°C for different times. a) As-decomposed microstructure of a $Mg(OH)_2$ crystal, b), c) and d) are the microstructures of the same crystal annealed for 90, 280 and 480 minutes, respectively.

Fig. 6: The line profiles and the superimposed small angle diffracted rings obtained from a) as-decomposed microstructure and b) crystal annealed at 700°C for 480 minutes.

Fig. 7: Averaged line profiles of power spectrums obtained from the digitized images shown in fig. 5 correspond to a) as-decomposed microstructure, b) annealed for 90 min at 700°C, c) annealed for 280 min at 700°C and d) annealed for 480 min at 700°C.

Fig. 8: Shows a sequence of micrographs of a MgO pseudomorph recorded at 900°C for different annealing times. a) The microstructure of a fully decomposed $Mg(OH)_2$ crystal viewed along [0001] direction immeadiately after decomposition. The same crystal annealed for 40 minutes b), 90 minutes c) and 120 minutes d).

Fig. 9: A video sequence showing the stages of growth of a cubic MgO crystal from the [111] oriented MgO pseudomorph shown in fig. 8 after annealing for 125 minutes at 900°C. a) 0 sec, b) 150 sec and c) 310 sec.

Fig. 10: Averaged line profiles of power spectrums obtained from digitized images shown in fig. 8.

Fig. 11: High resolution electron micrographs of MgO nanocrystals from a) as-decomposed microstructure and b) the MgO pseudomorph annealed at 700°C for 480 minutes, showing the crystallite stacking in [100] projection.

Fig. 12: High resolution electron micrographs of MgO nanocrystals in [110] projection from a) as-decomposed microstructure and b) crystal annealed at 700°C for 480 minutes.

Fig. 13: a) A micrograph showing the region where disintegration of MgO pseudomorph, nucleation, growth and coalescence of new MgO crystals have taken place. b) A region away from fig. a shows the MgO particles formed by migration.

Fig. 14: Microstructures of MgO pseudmorphs showing the effect of electron beam heating during high temperature annealing. The micrographs on the left show the microstructures of MgO pseudomorphs not affected by the high energy electron beam and on the right show the microstructures of MgO pseudomorphs observed during HVEM examination. The micrographs were recorded after annealing at 350°C for 60 minutes a,b), 700°C for 480 minutes c,d) and 900°C for 240 minutes e,f).

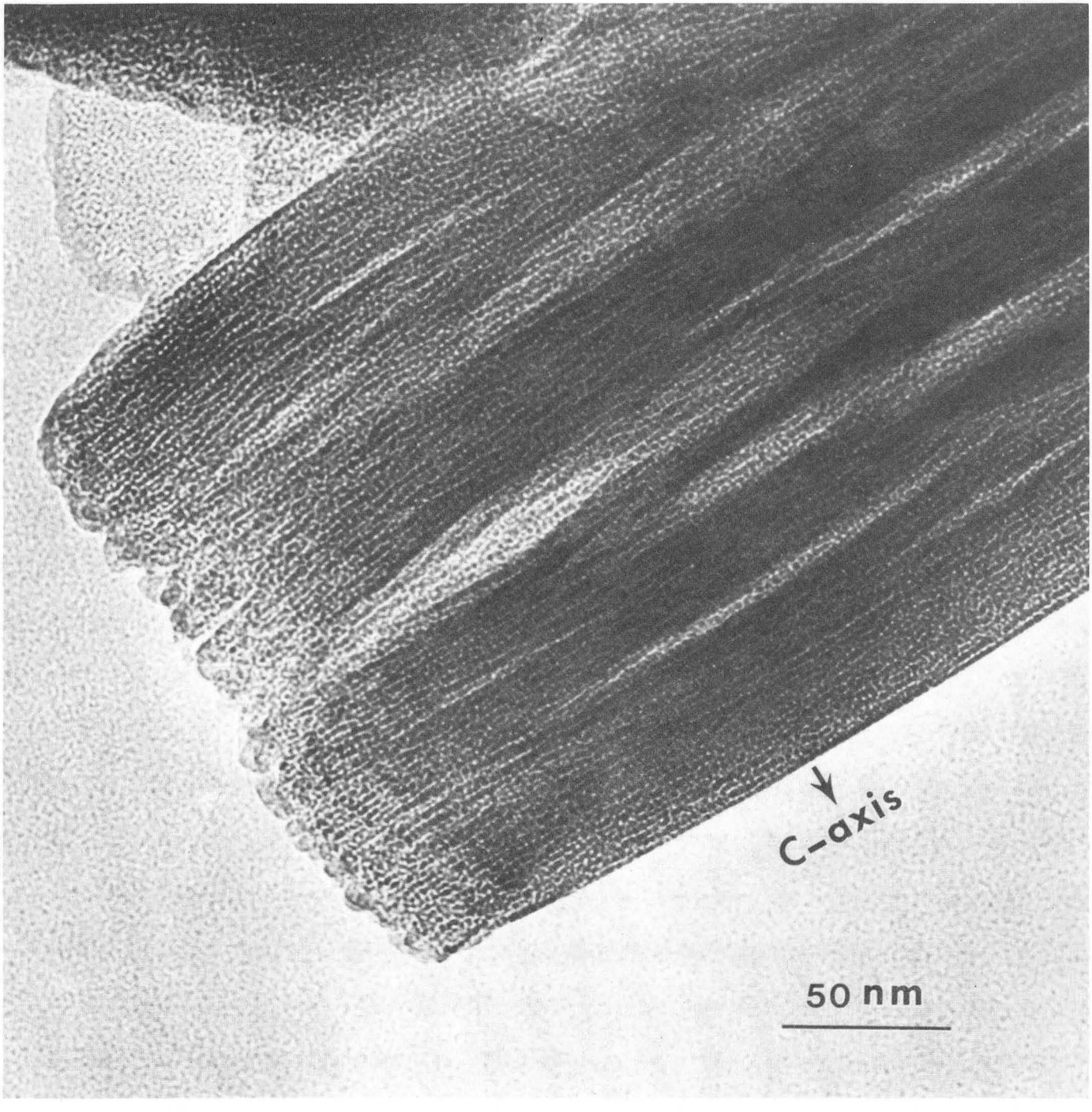

XBB 908-6550

Figure 1

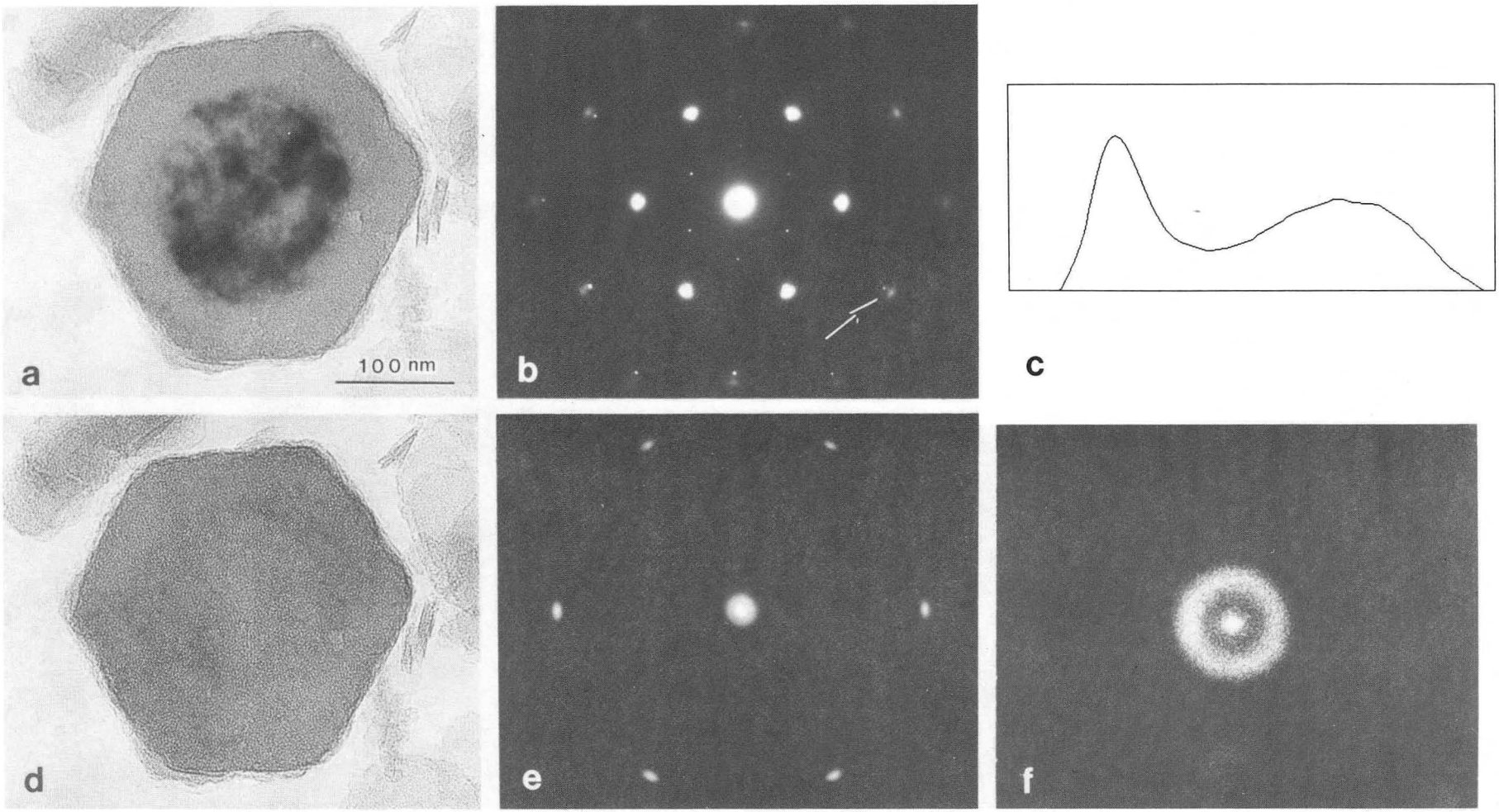

XBB 908-6557

Figure 2

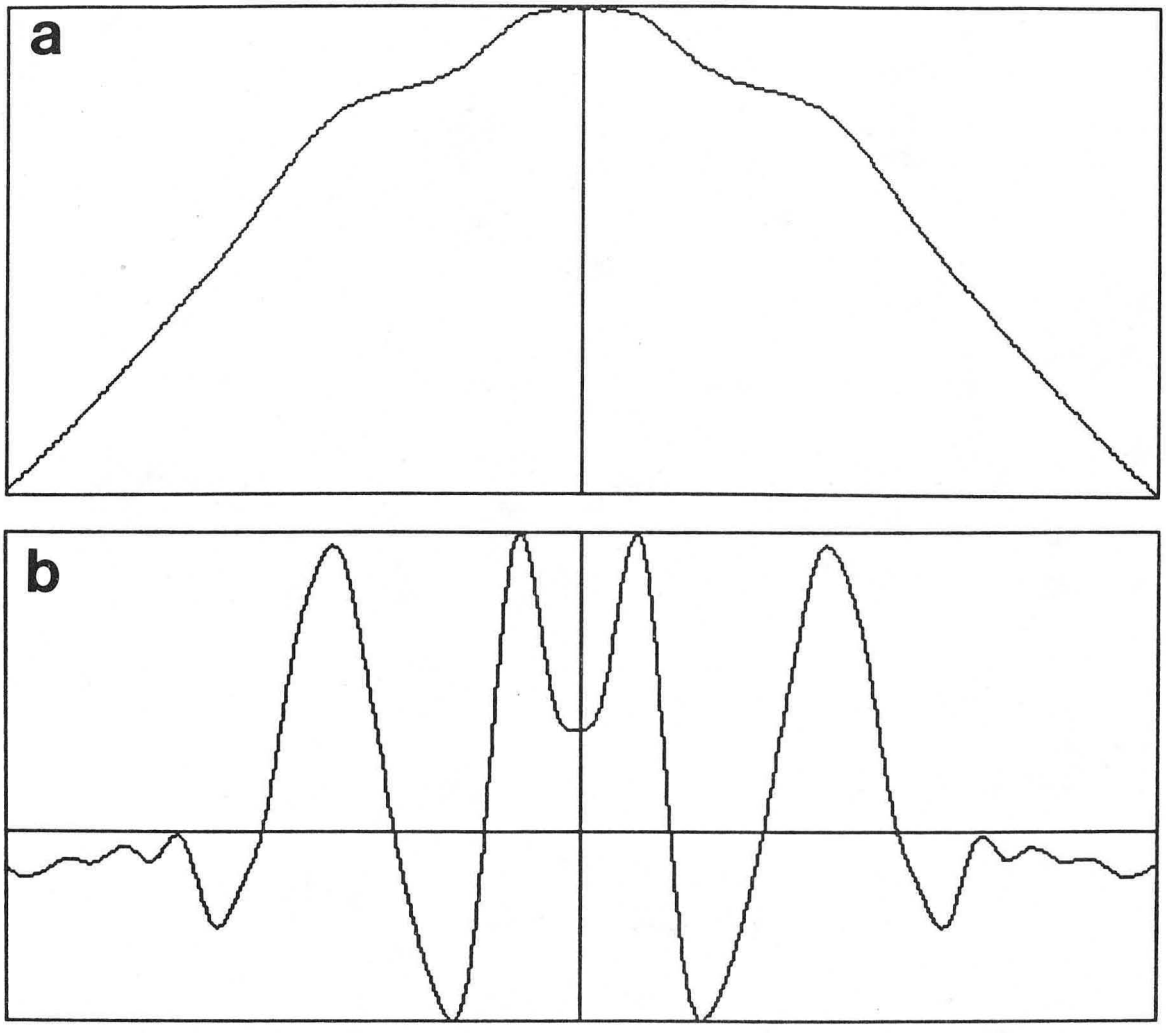

XBL 908-2813

Figure 3

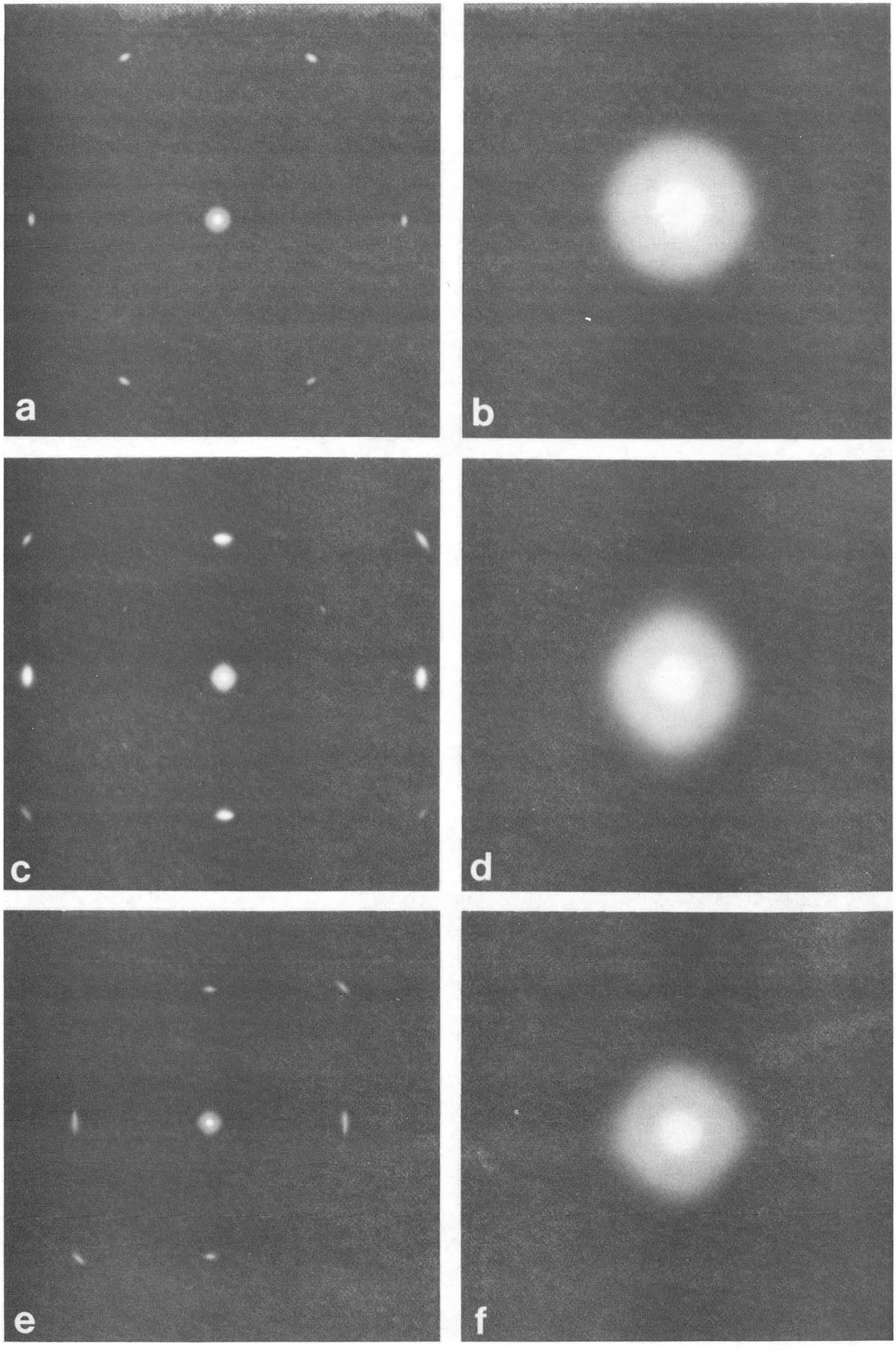

Figure 4

XBB 908-6549

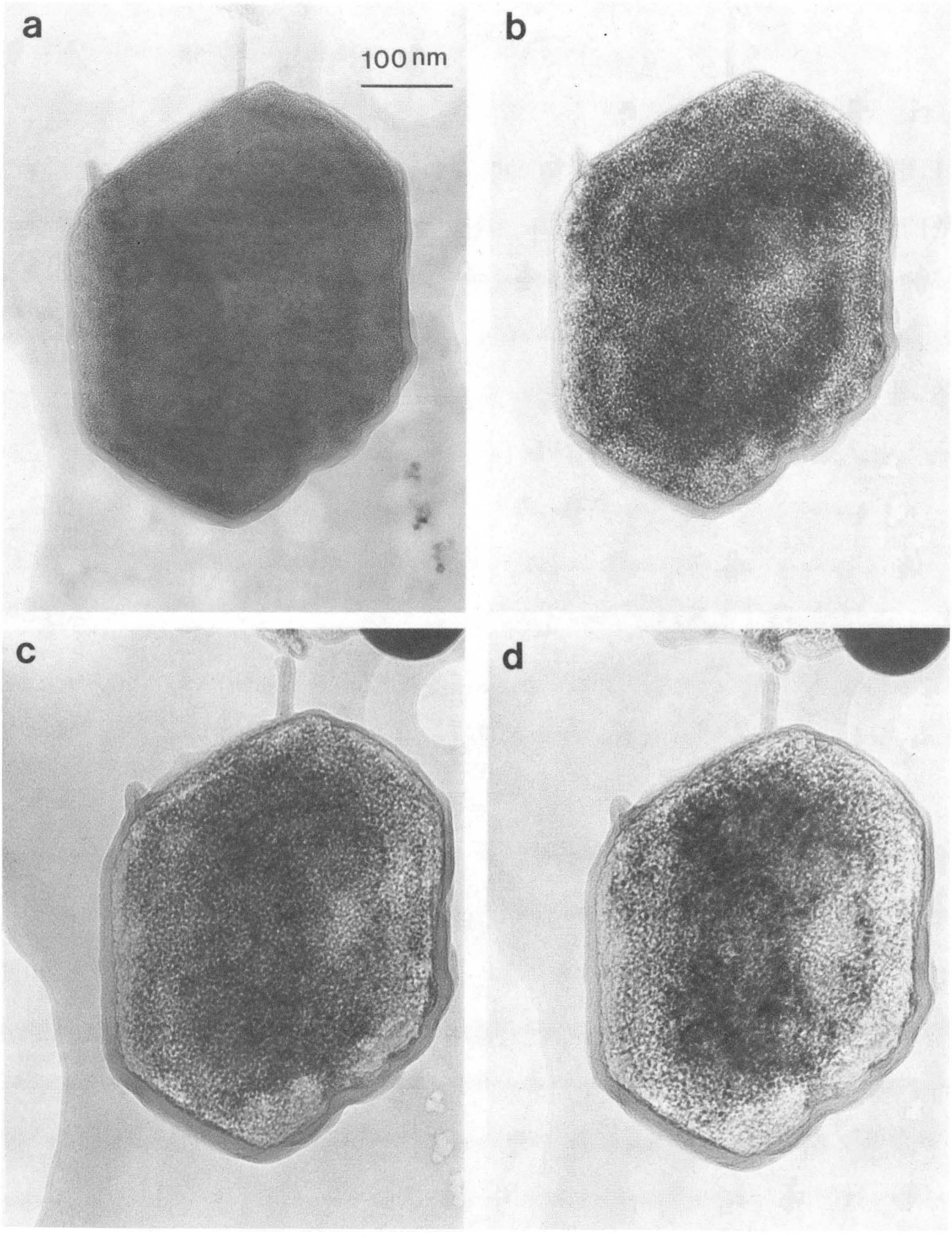

XBB 908-6548

Figure 5

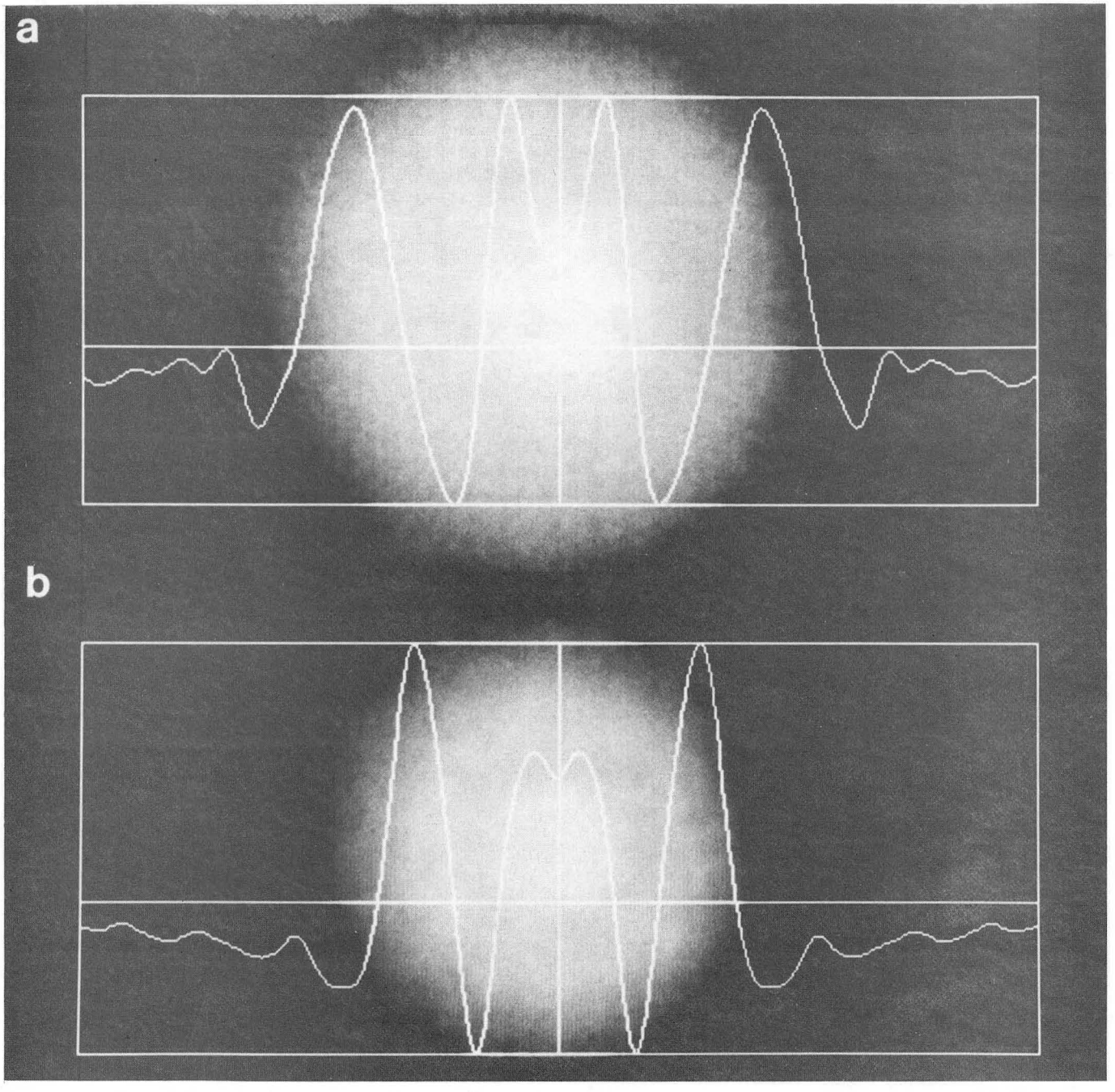

XBB 908-6547

Figure 6

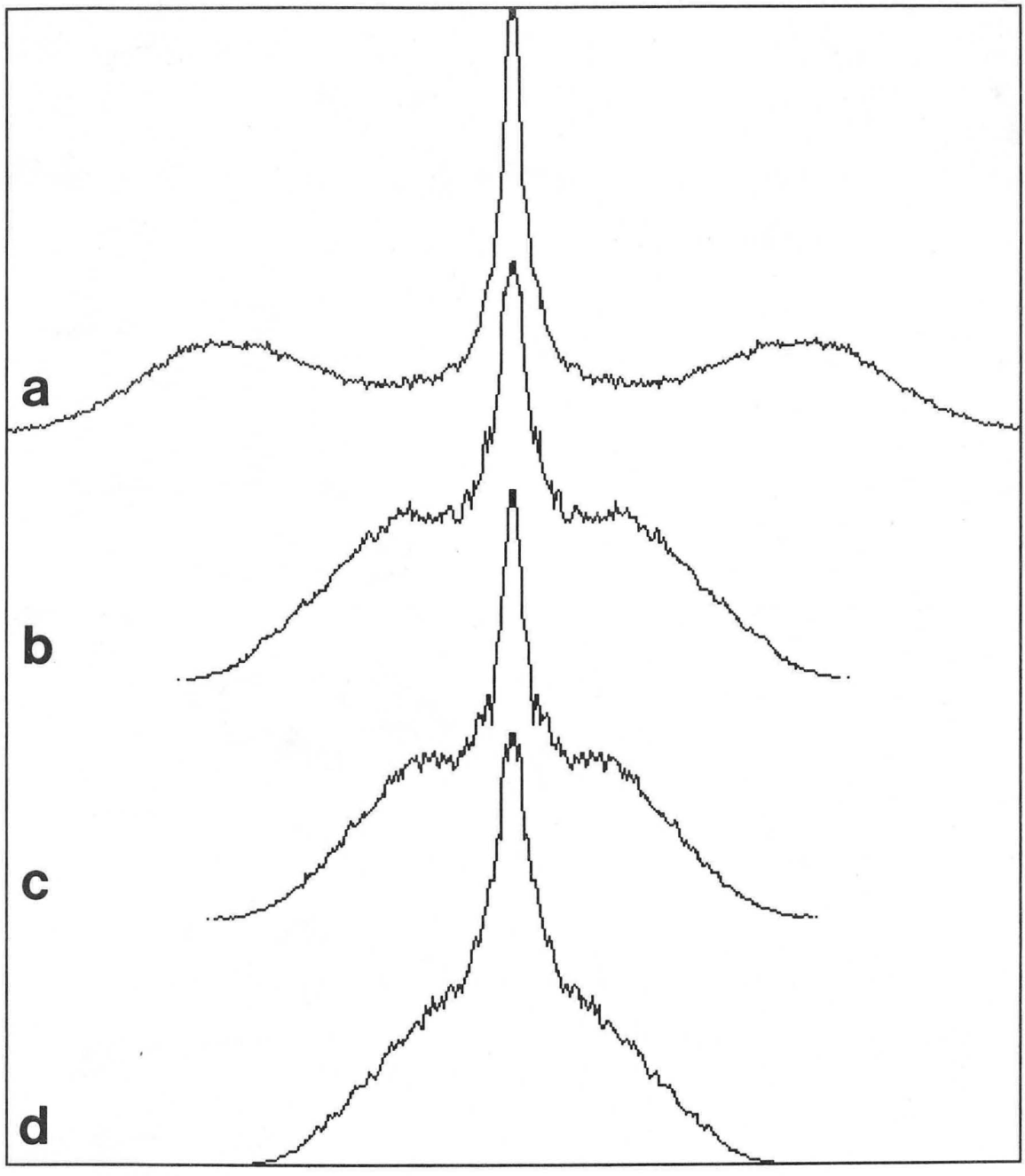

Figure 7

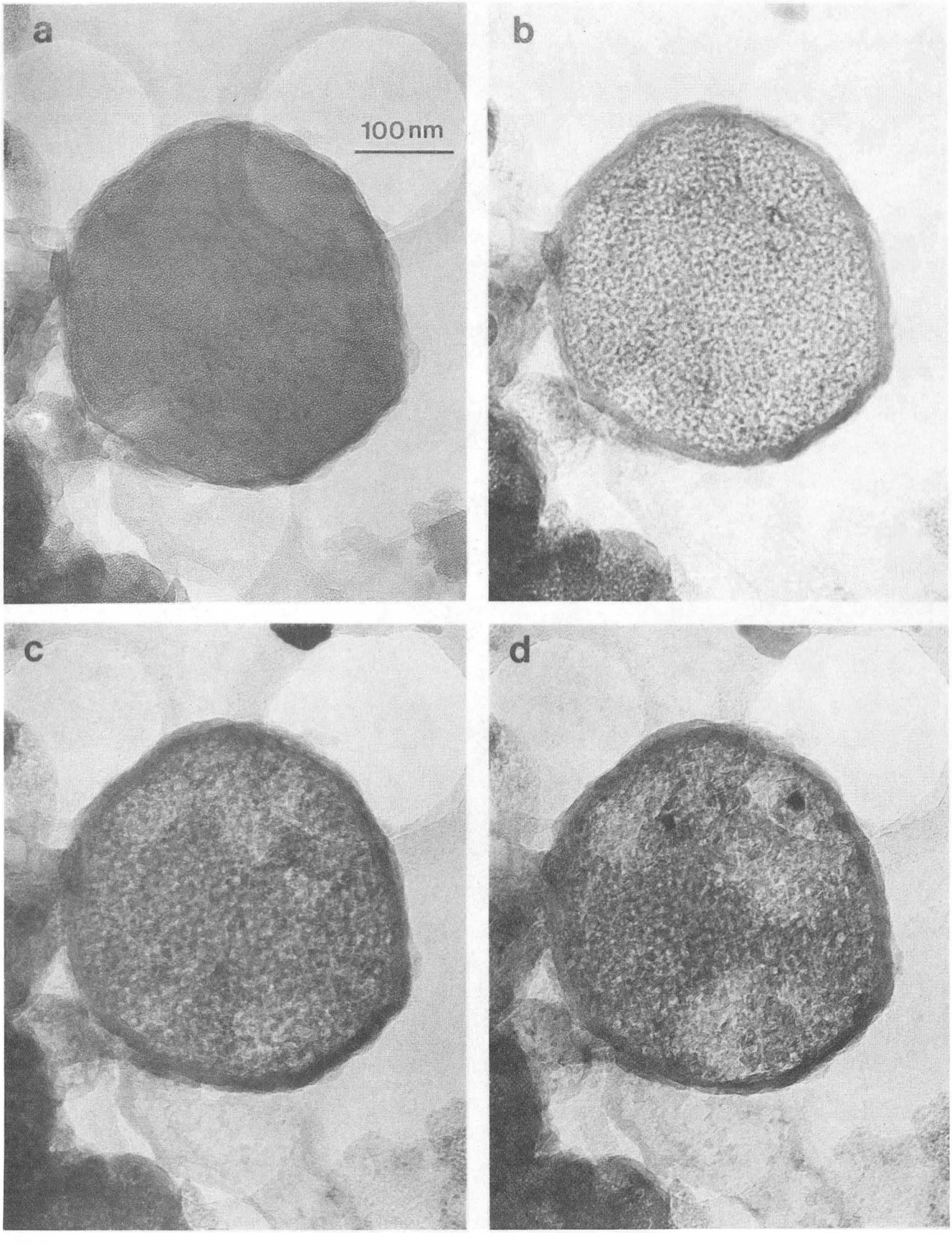

Figure 8

XBB 908--6555

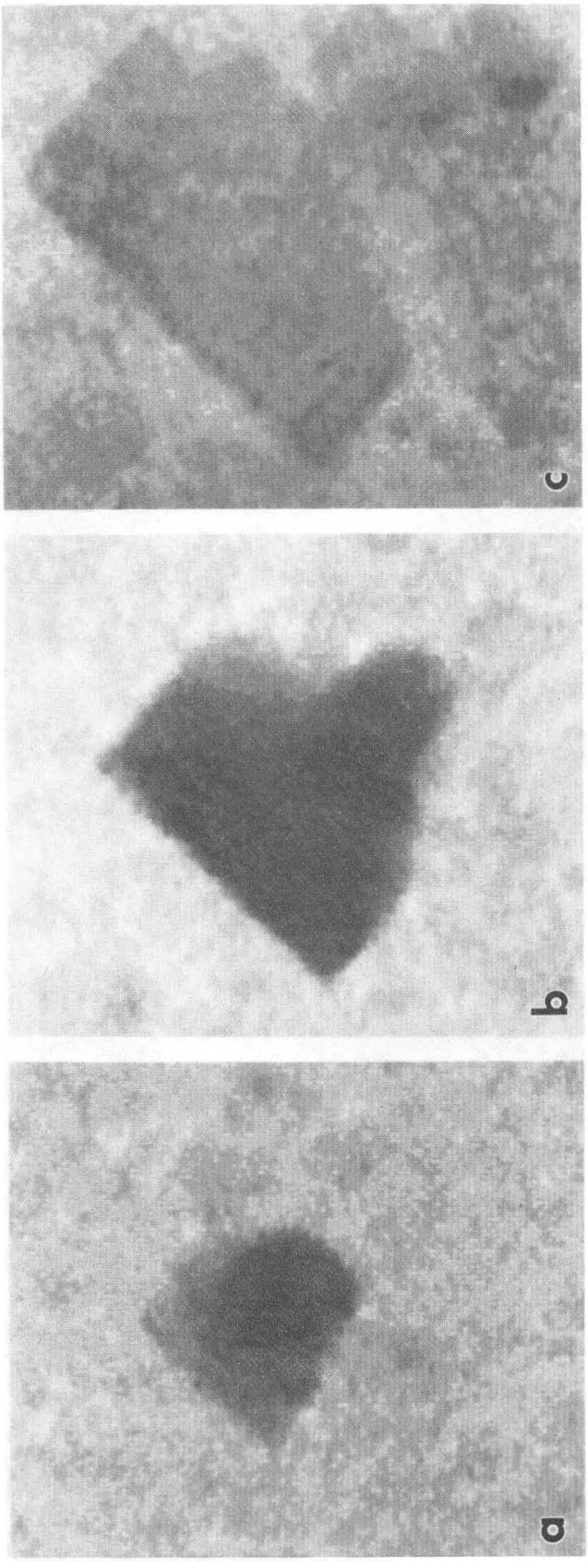

XBB 908-6553

Figure 9

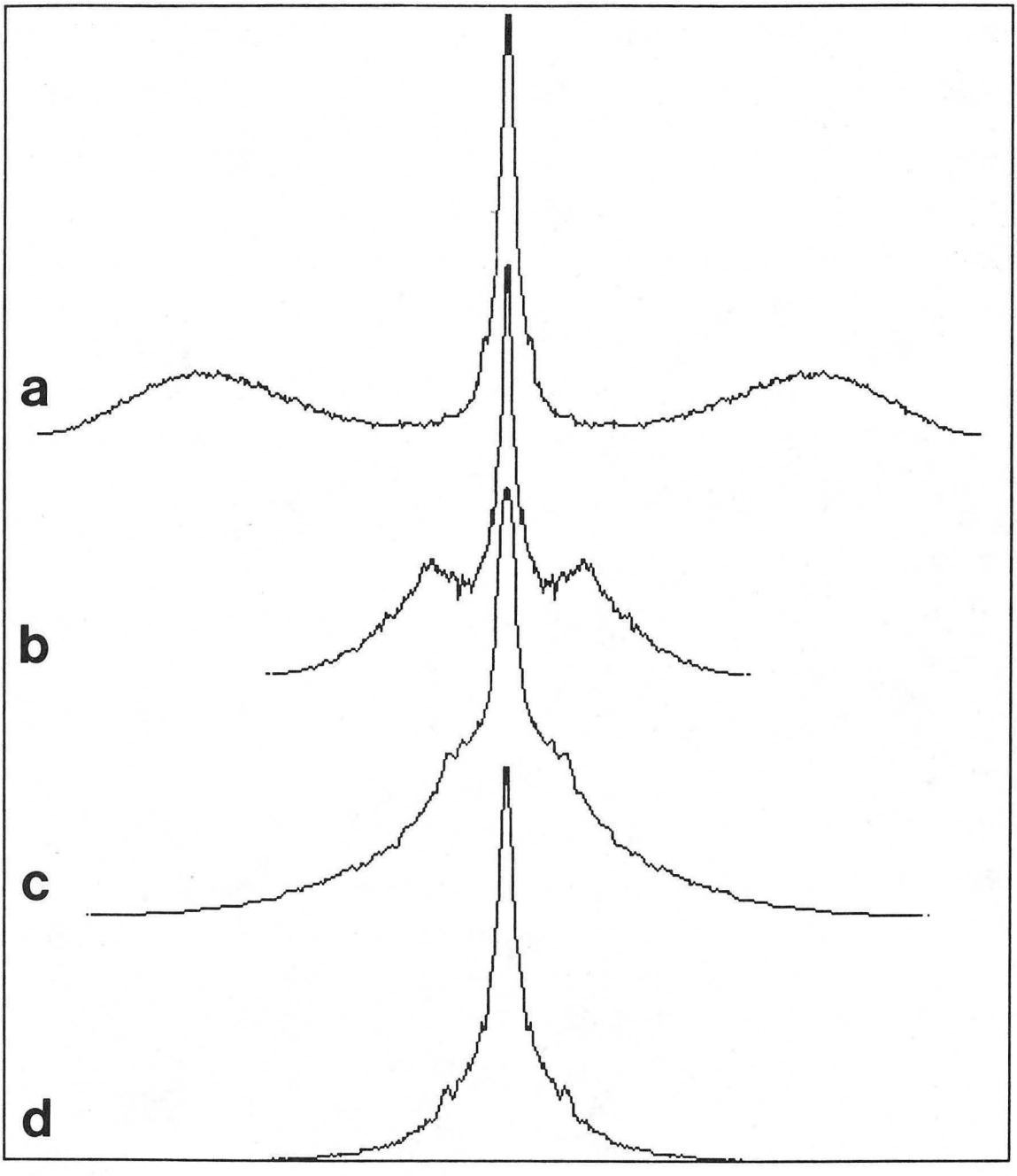

XBL 908-2814

Figure 10

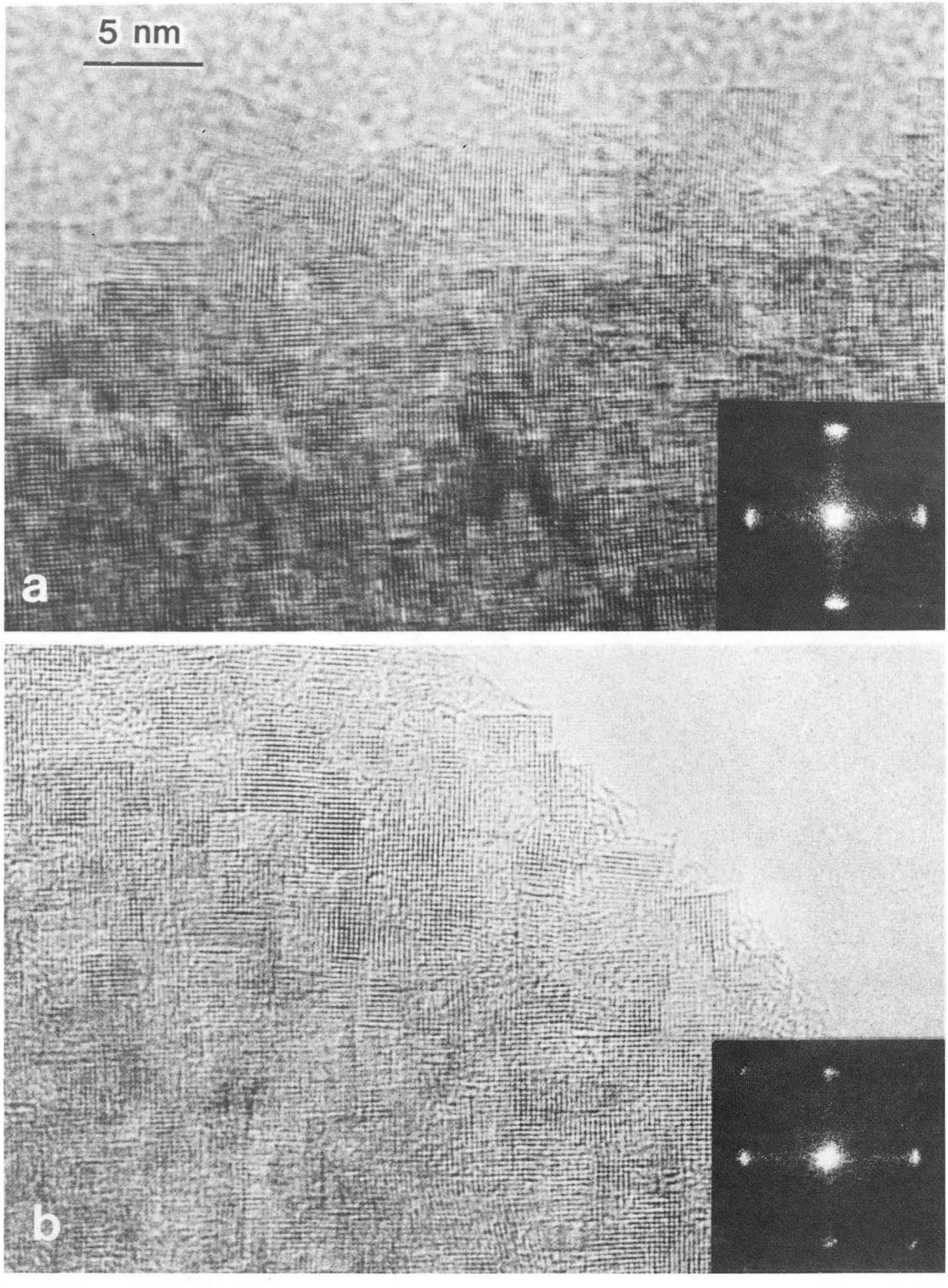

XBB 908-6551

Figure 11

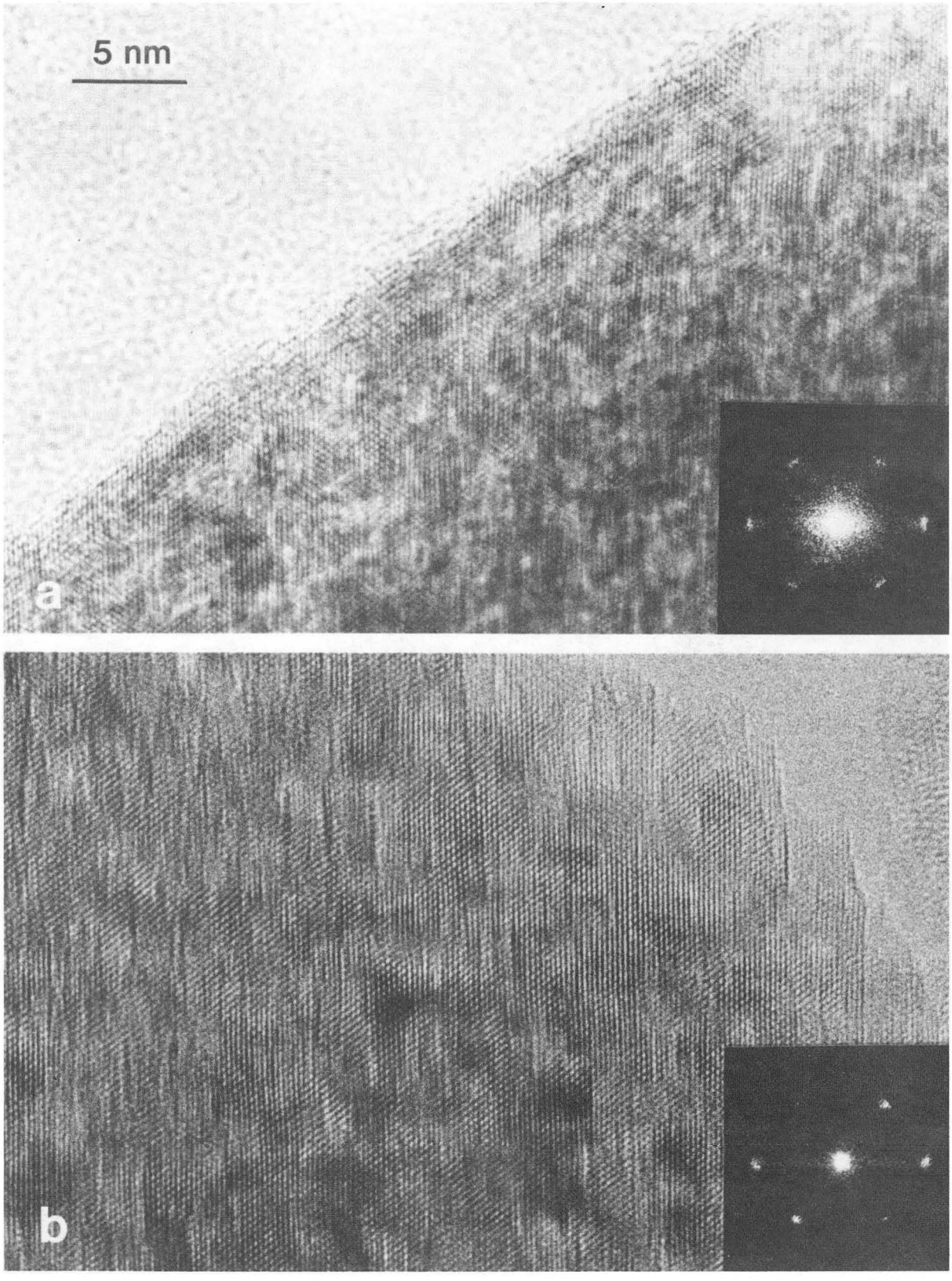

XBB 908-6552

Figure 12

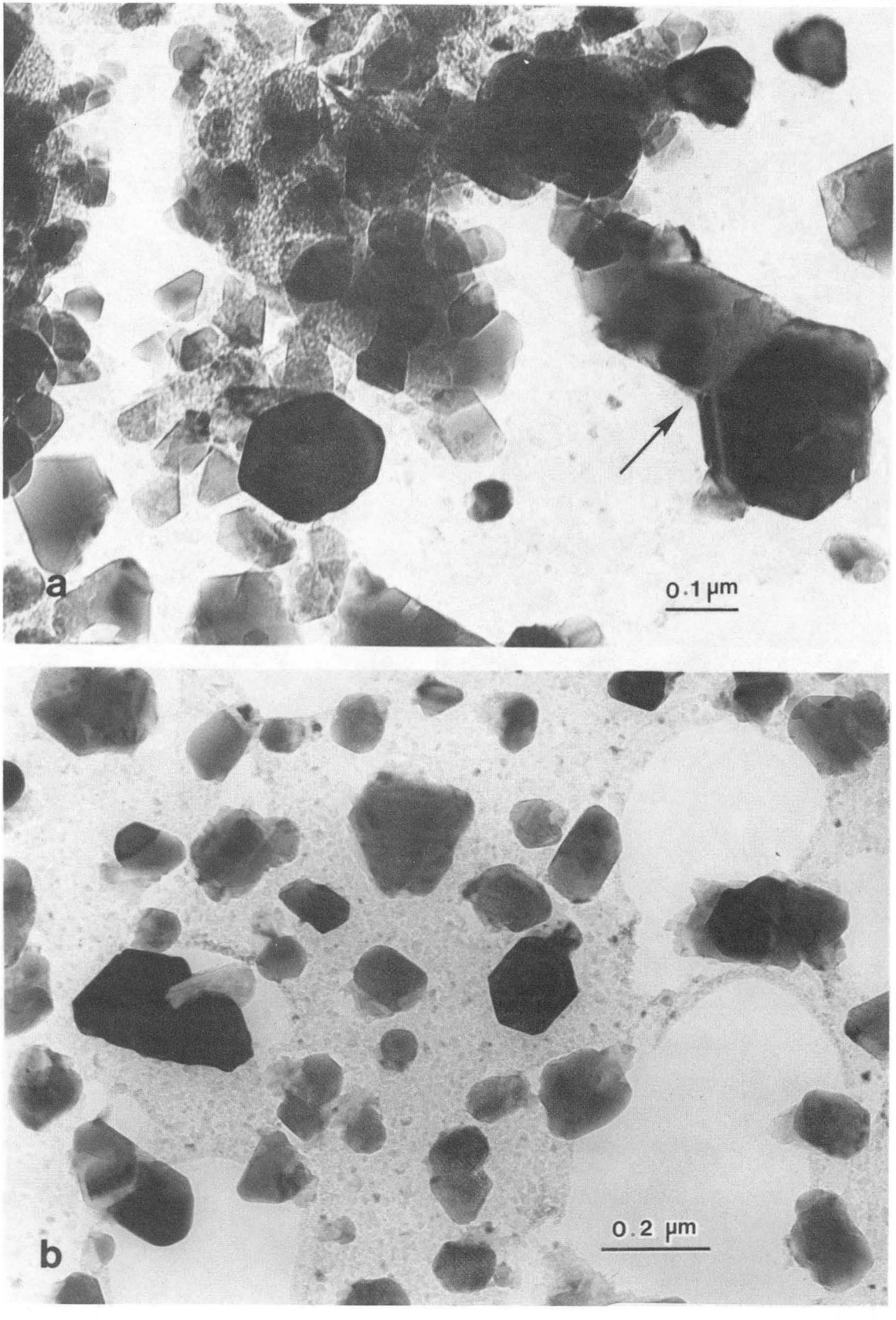

XBB 908-6554

Figure 13

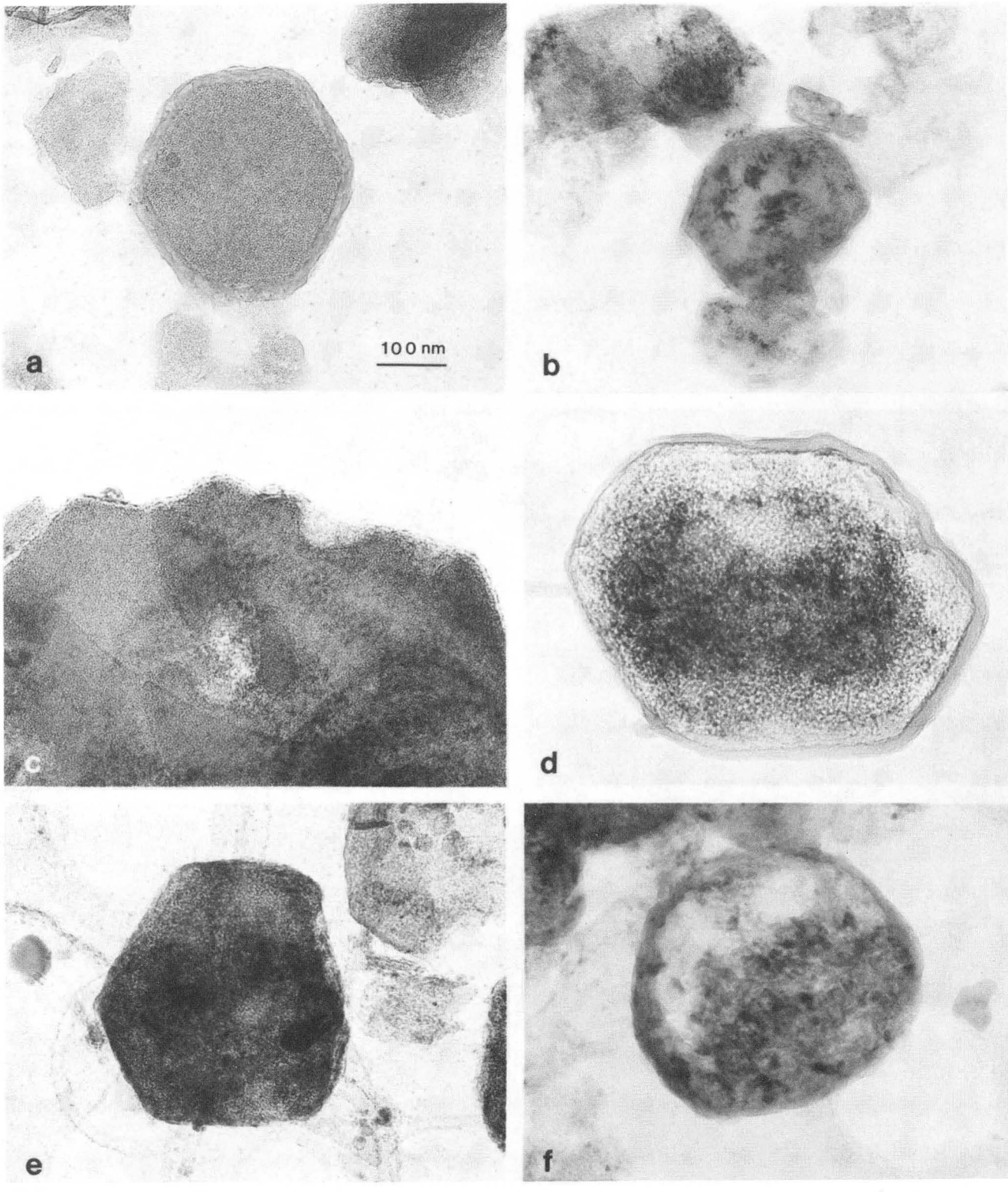

XBB 908-6556

Figure 14

LAWRENCE BERKELEY LABORATORY
UNIVERSITY OF CALIFORNIA
INFORMATION RESOURCES DEPARTMENT
1 CYCLOTRON ROAD
BERKELEY, CALIFORNIA 94720